Kinetics of Adsorption and Desorption of PEO−PPO−PEO Triblock Copolymers on a Self-Assembled Hydrophobic Surface

Pietro Brandani*,† and Pieter Stroeve*

Department of Chemical Engineering and Materials Science, University of California, Davis, One Shields Avenue, Davis, California 95616

Received February 28, 2003; Revised Manuscript Received August 15, 2003

ABSTRACT: We report on the kinetic behavior of adsorption from solution of a family of triblock copolymers, copoly(ethylene oxide−propylene oxide-ethylene oxide) (PEO−PPO−PEO), on a gold surface modified by a methyl-terminated, self-assembled monolayer (SAM) of a long-chain alkanethiol ($CH_3(CH_2)_{10}$-SH). We monitored the kinetics with a surface plasmon resonance (SPR) technique, whose fast time resolution (0.1 s) allowed us to follow the evolution of these systems even for characteristic times of a few seconds. The data were analyzed in the context of a mass transfer corrected Langmuir kinetics model. While the model is only able to reproduce the observations for either very dilute solutions or the initial stages of the process, it nevertheless allows us to discriminate the onset of the different mechanisms of adsorption. This study shows that, for a series of compounds with the same length of the PPO block, the intrinsic kinetics of the adsorption process is affected by the relative balance of the hydrophilic and hydrophobic content within the copolymer: higher hydrophobic content leads to enhanced adsorption rates past the critical micelle concentration (cmc). This is consistent with observations from our earlier study on the morphology of the polymer-coated surfaces by atomic force microscopy.

Introduction

Understanding the modality of interactions between polymers and surfaces is fundamental in trying to fulfill the goal of designing and creating functional adsorption-driven self-assembled nanostructures.[7,25,27] In this paper we report on the intrinsic kinetics of adsorption and desorption of a family of triblock copolymers, copoly-(ethylene oxide−propylene oxide−ethylene oxide), on a model hydrophobic surface. (The copolymers are commonly designated $PEO_nPPO_mPEO_n$; we shall use the simplified notation $E_nP_mE_n$ for the remainder of the paper.)

Various experimental techniques can be applied to study adsorption kinetics, including ellipsometry,[24] Brewster-angle reflectivity,[15] total internal fluorescence spectroscopy (TIRF),[16] attenuated total reflection infrared spectroscopy (ATR-FTIR),[14] and flow cytometry.[1] We have opted to probe our surfaces with a surface plasmon resonance spectroscopy (SPR) apparatus. SPR allows in-situ, nondestructive sampling of the deposition process in its native environment. Similarly, the species of interest retain their native physical characteristics since they do not need to include or be modified to include additions to their structure such as light-absorbing chromophores or radioactive labeling moieties. However, the most important consideration from the standpoint of our study is that SPR allows a time resolution (0.1 s) that is at least an order of magnitude faster than what can be achieved with the other techniques. We have already examined the equilibrium properties by SPR and the structure of the deposited layers of a selected number of systems by atomic force microscopy (AFM) in a previous publication.[6]

Green et al. have previously reported on the subject of PEO−PPO−PEO adsorption on a planar hydrophobic surface.[17] They were able to highlight important qualitative trends, notably the relative impact of the PPO and PEO blocks on the adsorbed amount at equilibrium and the greater rates of adsorption for micellar solutions over nonmicellar solutions for copolymers that have a higher content of PPO over PEO. However, the apparent lack of high time resolution in the SPR apparatus, the absence of a quantitative rendering of the SPR response curves, and, most importantly, the absence of an analysis of the flow conditions and their influence on the outcome of the experiments have precluded these authors from providing a more detailed and accurate picture of the kinetics of the adsorption process for this system.

The aim of this study is to investigate the influence of copolymer architecture on the kinetics of adsorption and desorption of PEO−PPO−PEO triblock copolymers on a model hydrophobic surface and supplement the experimental observations with theoretical analysis in order to better elucidate the dynamics in play at the different time scales typical of these polymer systems.

The contents of the paper are as follows: We first present kinetics data and discuss pertinent modeling issues. We find that, for this series of Pluronics that have similar hydrophobic cores, the kinetic behavior falls into two classes that depend on the relative balance of the hydrophilic and hydrophobic contents. We then focus our attention on P103 ($E_{17}P_{60}E_{17}$, a more hydrophobic species) and P105 ($E_{37}P_{56}E_{37}$, a more hydrophilic species) by examining the detailed evolution of the adsorbed amounts and comparing it against the predictions of a Langmuir kinetics model corrected for the effects of mass transfer. This approach is useful in describing the initial stages of the kinetic experiments while the surfaces are still relatively unoccupied, and it clarifies the emergence of the polymer asymptotic

† Present address: Center for Biophotonics Science & Technology, University of California, Davis, 4800 2nd St, Suite 2600, Sacramento, CA 95817.

* To whom correspondence should be addressed: Tel 530-754-7212, Fax 530-752-2444, e-mail pbrandani@ucdavis.edu; Tel 530-752-8778, Fax 530-752-1031, e-mail pstroeve@ucdavis.edu.

10.1021/ma034268x CCC: $25.00
Published on Web 10/30/2003

behavior as the model sharply diverges from the experimental observations at the long time scales.

Experimental Section

Materials. The Pluronic surfactants P123 ($E_{19}P_{69}E_{19}$), P103 ($E_{17}P_{60}E_{17}$), P104 ($E_{27}P_{61}E_{27}$), P105 ($E_{37}P_{56}E_{37}$), and F108 ($E_{132}P_{50}E_{132}$) were a gift from BASF Corp. Deionized water (18.2 MΩ cm) from a NanoPure system (Barnstead, IA) was used to prepare the polymer solutions and to run the water rinsing steps in the experiments. All solvents and chemicals were of analytical grade. The ethanol used in thiol solution preparation was absolute 200 proof (Gold Shield Chemical Co., Riverside, CA). Undecanethiol used for the formation of monolayers on gold was purchased from Aldrich-Sigma.

Preparation of Gold Slides. We have used high refractive index LaFSN9 glass slides (Schott, Germany) as substrates for SPR experiments and mica sheets as substrates for AFM. Gold of 99.999% purity was used to coat the glass substrates by sputtering. About 50 nm of gold was deposited on the glass slides by heating a gold target in a crucible with an electron beam at a pressure below 5×10^{-6} Torr, with a gold deposition rate of 0.2 Å/s. Finally, the gold slides were annealed at 650 °C for 30 s to minimize the surface roughness of the gold.[19]

Preparation of Thiol Monolayers. When gold is exposed to a thiol solution, self-assembled monolayers form spontaneously. Typically thiolate self-assembled monolayers can be modified through syntheses of alkanethiols with varying terminal groups to adjust surface energies and charge.[9] In this study we have used a methyl-terminated SAM to achieve a model hydrophobic surface. Self-assembly of the thiol monolayers was achieved by injecting a 5 mM undecanethiol solution in alcohol into the flow cell containing a freshly prepared gold slide. The solution was allowed to react with the gold for at least 16 h, a time considered to be adequate for SAM formation, and then rinsed with at least 20 mL of ethanol at a flow rate of 5 mL/min and at least 200 mL of water at a flow rate of 10 mL/min to reach complete removal of thiol residue. SPR kinetics experiments showed that more than 99% of undecanethiolate SAM formation was complete within 16 h.

Construction of Flow-Cell Apparatus. A narrow slit cross-section flow cell was fabricated from Teflon and was lined with a BUNA-N O-ring to provide for a watertight seal. The flow channel was 14 mm wide and 75 mm long. The gap between the glass slide and the Teflon wall was 0.25 mm. The measurement target was 40 mm from the inlet, and the laser target had a cross-sectional area of about 2 mm^2. The target length to inlet gap ratio is 160, large enough to give fully developed, laminar flow at the measurement location. Solutions were pumped using 100 mL Popper & Sons Inc. glass syringes in a Cole-Parmer 74900 syringe pump and a peristaltic MasterFlex Digi-Staltic 77340-00 pump provided by Cole-Parmer. For most experiments the cell was operated in the laminar regime at typical Reynolds numbers around 200.

Surface Plasmon Resonance Spectroscopy. A more extensive description of SPR is given in our previous publication.[6] Briefly, for the experiments, we used a SPR apparatus in the Kretschmann configuration.[21] A LaSFN9 prism was placed over a gold-coated LaSFN9 glass slide, and monobromonaphthalene (Bellingham & Stanley Ltd., United Kingdom) was used as a matching fluid. Monochromatic p-polarized light from a 633 nm laser was used as the light source. The intensity of the reflected light was captured by a photodiode whose output was sent to a lock-in amplifier (Stanford Research Systems, Sunnyvale, CA) and on to a PC for data handling and storage. A $\theta-2\theta$ goniometer (Huber GmbH, Germany) acted on by a stepper motor capable of 0.001° increments (Blake Industries, Inc., Scotch Plains, NJ) was used to perform scans of the intensity of the reflected light as a function of the incident angle. The SPR curves (reflectivity vs internal angle) were modeled using the characteristic matrix formalism for homogeneous stratified dielectric media.[5,18] A fitting procedure was used in which refractive indices for all layers as well as thicknesses for the inner layers were fixed and the thickness of the last deposited layer calculated to give the least-squares match for the experimental SPR curves. We followed the kinetics by fixing the detector at a given angle and monitoring the reflectivity as a function of time. Typically, this angle is chosen 0.5°−2° less than the resonance angle so that changes in reflectivity are linearly related to the shift in resonance angle or, alternatively, to the change in adsorbed layer thickness. The sampling time was 0.1 s. Adsorption and desorption kinetics were complemented with full SPR angular scans before and after each kinetic run. At higher concentrations of polymer in solution the change of reflectivity for an adsorption or desorption experiment is not only due to the changes in the adsorbed layer, but it is also affected by the concentration related change in refractive index in the bulk solution. We took this concentration effect into account by calculating the extent of bulk fluid contribution with the optical model and by subtracting it from the kinetics curves. Finally, all measurements were performed at room temperature.

Polymer Excess Surface Concentration. Assuming changes in index of refraction are linear with respect to changes in bulk concentration of the solute, one can use the following relation to determine the excess surface concentration of the adsorbed species:[11]

$$\Gamma = \frac{d_f(n_f - n_s)}{dn/dc}$$

where Γ is the block copolymer excess surface concentration (μmol/m^2), d_f is the film thickness (nm), dn/dc (M^{-1}) is the incremental change in the refractive index of solution with the increase in surfactant concentration, n_f is the index of refraction of the polymer film, and n_s is the refractive index of pure solvent, in our case water. The adlayer thickness d_f calculated by the SPR model is strongly dependent on the choice of film refractive index n_f; however, the optical thickness (i.e., the product in the numerator of eq 1) and consequently the adsorbed amount are nearly invariant.[12,28] The error on the calculated excess surface concentrations assuming a constant optical thickness is below 10%.

Refractive Index Measurements. Refractive index measurements of ethanol, ultrapure water, and aqueous Pluronic solutions were made on an Abbe 60 refractometer (Bellingham & Stanley Ltd., England) using a sodium spectral lamp as the light source ($\lambda = 589.3$ nm). Refractive index of polymer varied linearly with concentration in the range used for this study. Values of the refractive index gradient dn/dc at 25 °C observed for P123, P103, P104, P105, and F108 were 0.13, 0.13, 0.13, 0.14, and 0.12 (±2%), respectively.

Results and Discussion

For the investigation we selected a series of Pluronics P123, P103, P104, P105, and F108 on a SAM formed from the deposition of undecanethiol on a gold surface. The last four elements in this series have an increasing content of the hydrophilic PEO block and an average content of 57 PO units per PPO block, while the first two have similar EO/PO ratio (EO/PO ∼ 0.56) but differing number of PO units in the PPO block: 69 vs 60 (Figure 1 and Table 1).

Adsorption and Desorption Kinetics. The outcome of an adsorption experiment is affected by the balance between the intrinsic rate of adsorption of the polymer onto the surface and the convective−diffusive rate of transport of the polymer across the liquid phase. Accordingly, one can envision two ideal limiting conditions that characterize this process: the diffusion-limited regime in which the surface acts as a perfect sink with intrinsic rates of adsorption that are many orders of magnitude higher than mass transport rates

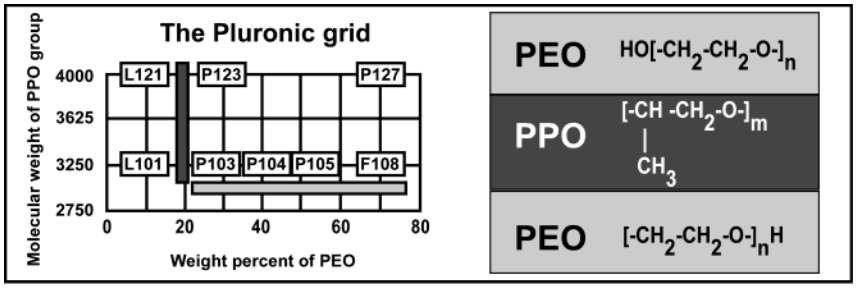

Figure 1. Characteristic grid for the identification of Pluronics: compounds on the same row have the same amount of PO, and compounds in the same column have similar EO/PO.

Table 1. Properties of Pluronics Selected for This Study

polymer	MW	m = no. of PO	n = no. of EO	cmc [μM][a]
P123	5750	69	2 × 19	30
P103	4950	60	2 × 17	168
P104	5900	61	2 × 27	530
P105	6500	56	2 × 37	385
F108	14600	50	2 × 132	3078

[a] Interpolated cmc data at $T = 25$ °C from Alexandridis et al.[2]

and the kinetic-limited regime in which the mass transport can be sustained at rates that are many orders of magnitude higher than intrinsic rates of adsorption. This is illustrated in the following simplified argument.[8] Assuming that a reversible first-order process describes the adsorption mechanism, we can write

$$\frac{d\Gamma}{dt} = k_{ads}(c^s - c^*) \tag{1}$$

where k_{ads} is the intrinsic rate of attachment, c^s is the so-called subsurface concentration, and c^* is the equilibrium concentration corresponding to a given value of $\Gamma(t)$. Likewise, assuming that we are past the initial transient and that the concentration gradient, which is the driving force in the transport process, varies very slowly in time (quasi-steady-state conditions), we can write

$$\frac{d\Gamma}{dt} = k_{trans}(c^b - c^s) \tag{2}$$

where k_{trans} is a mass transport rate coefficient, which depends on the diffusion coefficient of the adsorbing species and the hydrodynamic conditions, and c^b is the concentration in the bulk solution. We can eliminate c^s by combining eqs 1 and 2 and substituting back into one of the original equations to obtain

$$\frac{d\Gamma}{dt} = \frac{c^b - c^*}{k_{ads}^{-1} + k_{trans}^{-1}} \tag{3}$$

When k_{ads}^{-1} is much smaller than k_{trans}^{-1}, we are in the mass transport limited regime. Vice versa, when k_{ads}^{-1} is much greater than k_{trans}^{-1}, we are in the kinetic limited regime. In principle, for a given polymer system, we can change the hydrodynamic conditions (increase the flow of solution through the cell) such that the mass transport contribution to the adsorption process becomes negligible, and the system's dynamic response is a manifestation of the intrinsic adsorption process kinetics.

Figure 2 illustrates an experimental example of this procedure.

The figure shows that for the low and high ends of the concentration range, and for both the adsorption and desorption runs, as we increase the Peclet number, or the flow rate, which is directly proportional to it, we observe that changes become progressively smaller and the response curves practically indistinguishable. In Figure 3, we look at one of the adsorption runs more closely. Jumps in the rate of adsorption at the start of the run and, subsequently, at the restart of the run after a syringe change indicate that mass transfer is likely to be influencing the process.

In fact, further analysis confirms that the initial stages of the adsorption runs are not kinetically limited and that we are in a regime where neither step is limiting. We begin our analysis by referring again to the kinetics shown in Figure 2a (the kinetics of adsorption of a 0.001 cmc P105 ($E_{37}P_{56}E_{37}$) solution). We can compare the observed initial rates of adsorption to the ones that can be calculated for an analogous ideal diffusion-limited system[22,23]

$$\frac{d\Gamma}{dt} = \frac{D}{\delta} c_{bulk} \tag{4}$$

where δ is the concentration boundary layer given by

$$\delta = \text{Gamma}[4/3] \times 9^{1/3}\left(\frac{Dx}{\gamma}\right)^{1/3} \tag{5}$$

For example, these equations (see the Appendix for nomenclature and details on calculations) give for our system an estimated δ of 20 μm and an estimated value of the initial rate of adsorption of 0.0071 μmol/(m^2 s) at $Pe = Pe_0$ ($Pe_0 = 1.785 \times 10^8$), whereas the observed experimental rate at is 0.0045 μmol/(m^2 s). The experimental value is clearly lower than the Lévêque prediction for a diffusion-limited system, even taking into consideration a 10% margin of error in the estimate of the diffusivity D and the probing spot x. In Figure 4, we show the experimental data in the context of the predictions of the Lévêque equation (dashed line) and a mass-transfer-corrected Langmuir model (solid line). The figure shows that, within the experimental error, the data are consistent with a mixed mode regime. Pressure drop limitations prevented us from running at higher Peclet numbers.

Next, we examine the adsorption data for the case at higher concentration ($c = 10$ cmc P105, Figure 2c). The Lévêque solution for the base case ($Pe = Pe_0$) predicts an initial rate of 71 μmol/(m^2 s). For this case, the convection−diffusion model in the diffusion-limited regime estimates an initial rate of adsorption of 1.4 μmol/(m^2 s). The reason for the apparent discrepancy is that the quasi-steady-state assumption contained in the Lévêque equation is not fulfilled, and the transient

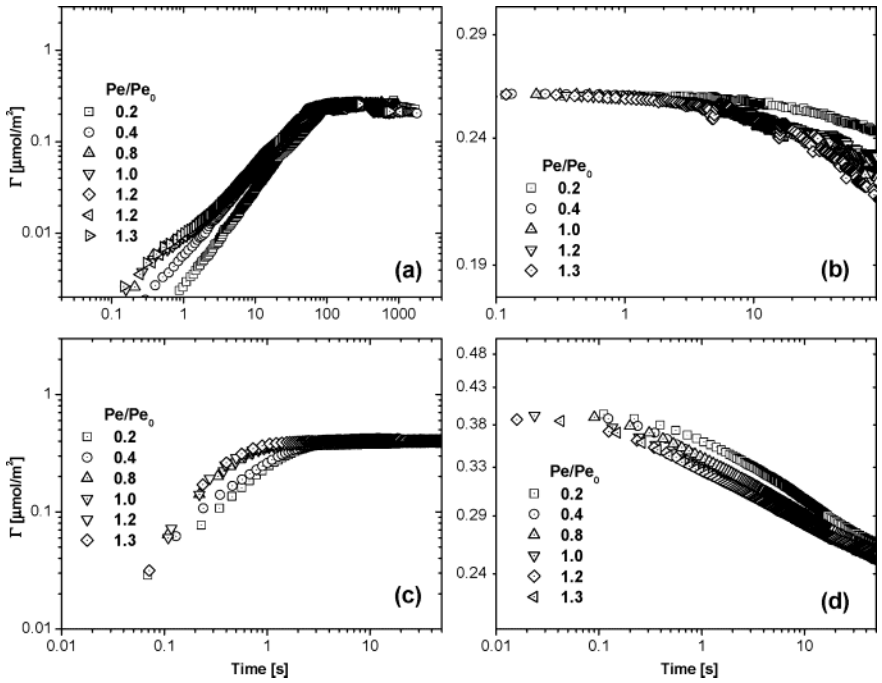

Figure 2. Log−log plot of the adsorption and desorption kinetics with increasing values of the Peclet number ($Pe_0 = 1.785 \times 10^8$) at the two limit concentrations for P105 ($E_{37}P_{56}E_{37}$). For 0.001 cmc P105: (a) adsorption, (b) desorption; for 10 cmc P105: (c) adsorption, (d) desorption. Heading in each figure shows change of bulk concentration where the symbol >> indicates change to.

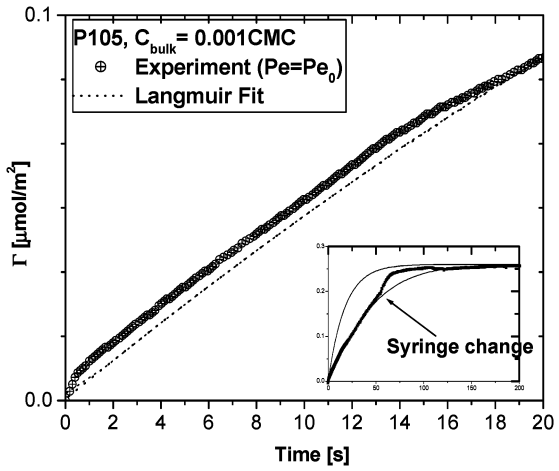

Figure 3. Adsorption kinetics for 0.001 cmc P105 ($E_{37}P_{56}E_{37}$) with $Pe = Pe_0$ ($Pe_0 = 1.785 \times 10^8$). The main graph highlights the system response in the beginning of the experiment; the inset gives the complete set of data for the experiment. Note that a temporary acceleration of the kinetics occurs at $t = 0$ s when the flow is started and at $t = 55$ s when the flow is stopped and then restarted after a syringe change. The dotted line represents the results of a fit using a Langmuir model corrected for mass transfer.

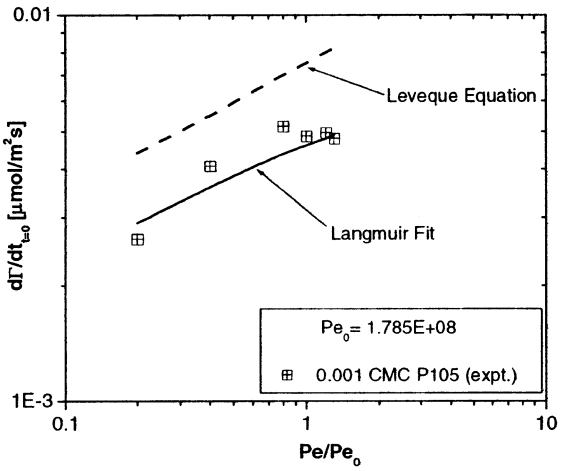

Figure 4. Experimental (squares), diffusion-limited (dashes), and mass-transfer-corrected Langmuir fit (solid line) initial rates of adsorption vs ratio of Peclet number to base case Peclet number, Pe_0 ($Pe_0 = 1.785 \times 10^8$), for the adsorption experiment shown in Figure 2a. Plots are on a log−log scale.

the term ($\partial\hat{c}/\partial\hat{t}$, eq 18 in the Appendix) cannot be neglected. The experimental data and the Langmuirian curve fit in Figure 5 show an initial rate of adsorption of about 0.8 μmol/(m^2 s). Again, the data are influenced by mass transport, but we are not at the diffusion-limited regime. The desorption runs show that the process is not mass transfer limited, and it is substantially slower than what the reversible Langmuir kinetics model predicts.

Despite the data being influenced by mass transfer, a definite trend emerges from the adsorption rates. Figure 6 and Figure 7 show the observed initial rates of adsorption and desorption, respectively. It is apparent that for P123 ($E_{19}P_{69}E_{19}$) and P103 ($E_{17}P_{60}E_{17}$) the initial rates change even past the cmc; for P104 ($E_{27}P_{61}E_{27}$), P105 ($E_{37}P_{56}E_{37}$), and F108 ($E_{132}P_{50}E_{132}$) the rates plateau near the vicinity of the cmc. These observations show that adsorption is unimer driven for the compounds with a higher hydrophilic content and that micellar adsorption plays a role for the ones with a higher relative hydrophobic content.

Overall these polymer systems are thought to undergo three distinct kinetic regimes:[13] an initial regime, at low coverages and short times, which is usually influenced by mass transfer; a second regime, at intermediate coverages and intermediate times, that is characterized by substitution of hydrophilic trains with hydrophobic chains at the surface; and finally an activation controlled barrier regime at high coverages and long times. The kinetic adsorption data for P103 ($E_{17}P_{60}E_{17}$) and P105 ($E_{37}P_{56}E_{37}$) are shown in Figure 8 and Figure 9,

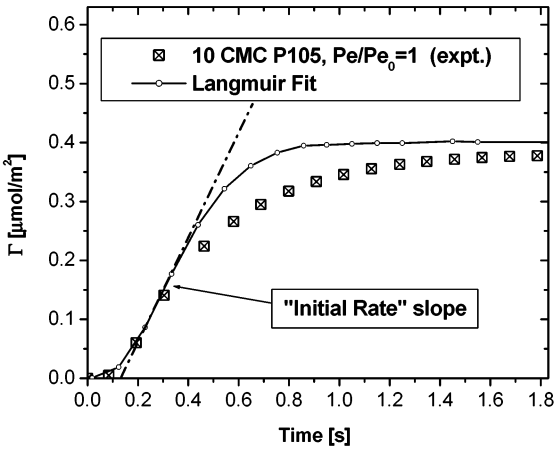

Figure 5. Adsorption kinetics for 10 cmc P105 ($Pe/Pe_0 = 1$, $Pe_0 = 1.785 \times 10^8$). Experimental (squares) and mass-transfer-corrected Langmuir fit (solid line). The dash−dot line indicates that the value of the slope at the inflection point is taken as the initial rate of adsorption.

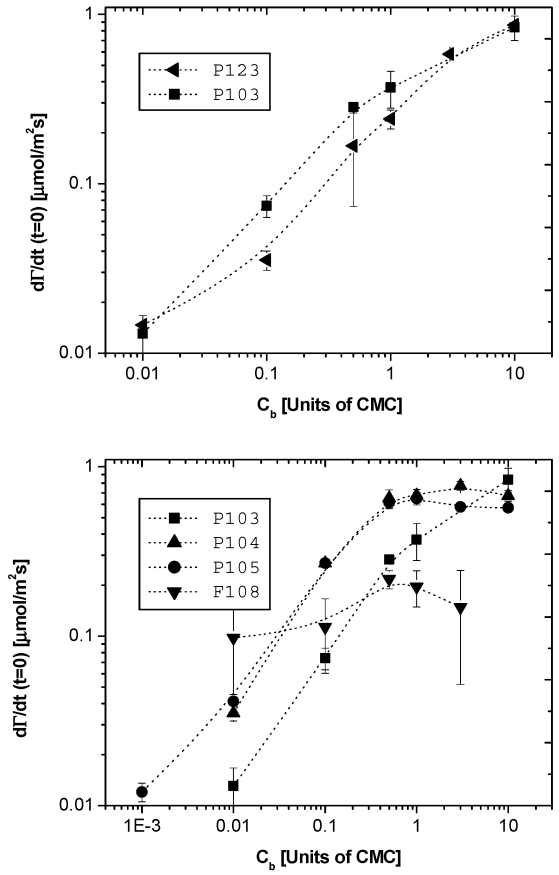

Figure 6. Log−log plots of the initial rates of adsorption for Pluronics with higher hydrophobic content (top panel) and for Pluronics with increasing hydrophilic content (bottom panel).

respectively. The data in Figures 8 and 9 have been plotted in terms of the function $f(t) = \Gamma(t\rightarrow\infty)/\Gamma(t) - 1$. The form of this function is particularly helpful in highlighting the behavior of the system at short and at long time scales. The dotted lines are the results of the mass-transfer-corrected Langmuirian fits. The solid lines are log−log fits of the dynamics at the long time step. Except at very dilute concentrations where the system exhibits Langmuir-like kinetics throughout the run (see Figure 8a), indeed we find evidence of a transition between mass-transfer-influenced kinetics

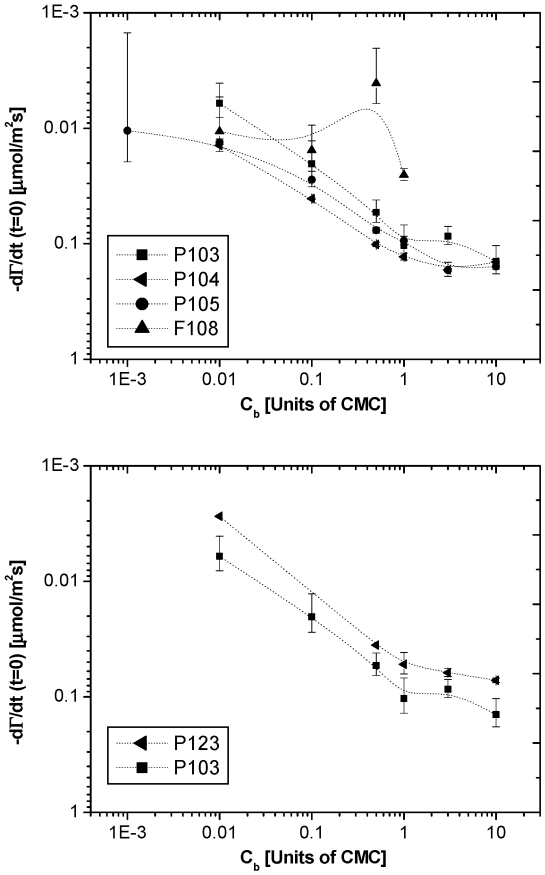

Figure 7. Log−log plots of the initial rates of desorption for Pluronics with higher hydrophobic content (top panel) and for Pluronics with increasing hydrophilic content (bottom panel).

and intrinsic kinetics that have a dependence that is linear with the logarithm of time. The dependence is consistent with the buildup of a brush, as shown by Johner et al.[20] The Langmuir-like model fails to capture the intrinsic kinetics for these copolymer systems, but it helps in identifying the boundaries of this transition. Looking closely at the logarithmic dependencies at the long time step, we again see a trend emerge. For P105 ($E_{37}P_{56}E_{37}$), the more hydrophilic compound, the slope of the log(t) line does not vary with concentration and has an average value of 0.5. P103 ($E_{17}P_{60}E_{17}$), however, also exhibits an average slope of 0.5 for values of the concentration at or below the cmc, but in contrast to the other species, it shows a marked increase of the slope past the cmc. As in the case of the initial adsorption rates, we again find an influence of micellar aggregation on the kinetics of the more hydrophobic compound.

Conclusions

We have studied the adsorption and desorption of kinetics of a family of triblock copolymers on a model hydrophobic surface. Employment of a fast time resolution surface plasmon resonance technique enabled us to follow the evolution of these systems even in fast kinetic regimes. Careful selection of the hydrodynamic conditions and modeling of the convective−diffusive contributions give an accurate and comprehensive picture of the intrinsic kinetic processes. Langmuir-like kinetics are observed only for very dilute solutions or in the initial stages of adsorption when the surfaces are still relatively unoccupied. The relative balance of the

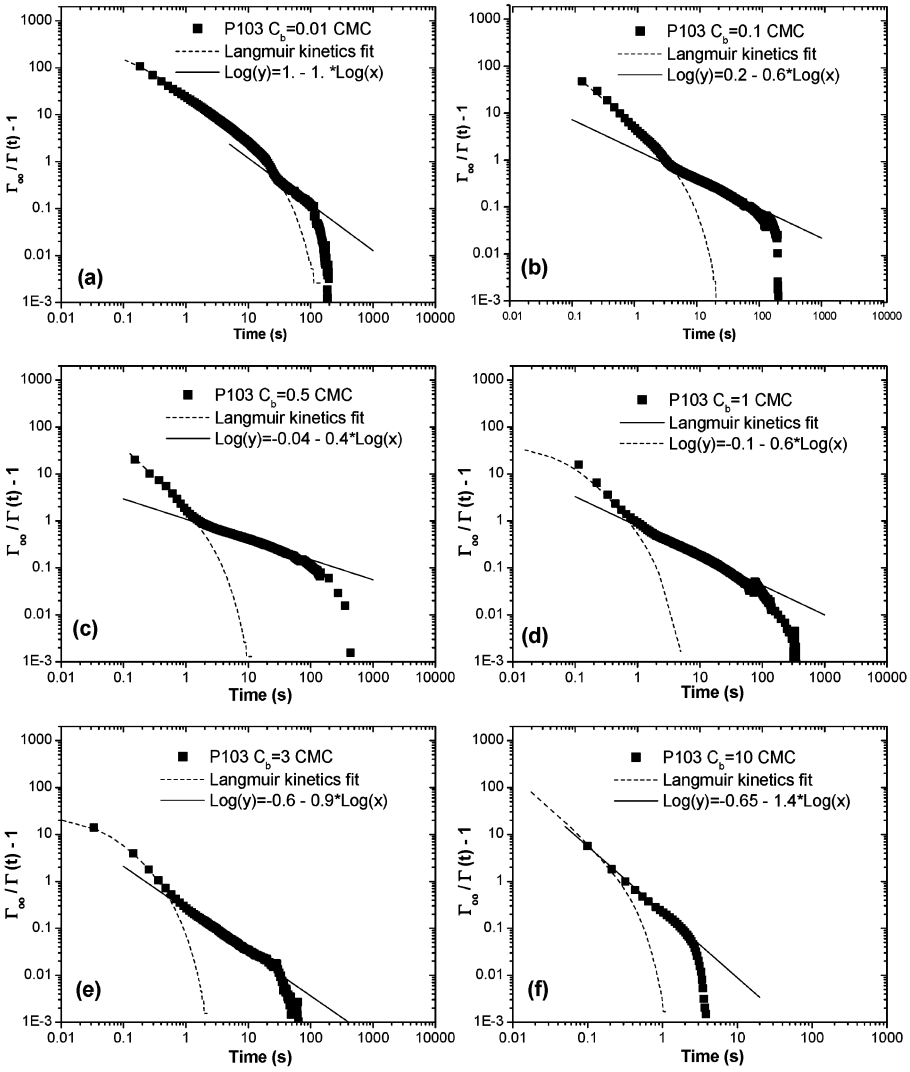

Figure 8. Comparison of the experimentally observed kinetics with the predictions of a Langmuir kinetics model (dashed curve) corrected to account for the effects of mass transfer for P103 ($E_{17}P_{60}E_{17}$) at (a) 0.01, (b) 0.1, (c) 0.5, (d) 1, (e) 3, and (f) 10 cmc concentration in the bulk solution. Solid line in each case highlights intermediate time asymptotic behavior. Plots are on a log−log scale.

hydrophilic and hydrophobic content within a copolymer species determines whether there is unimer driven adsorption or whether micelles play a role.

Appendix

Concentration Boundary Layer. We can combine eqs 4 and 5 and obtain the Lévêque equation:

$$\frac{d\Gamma}{dt} = \frac{D}{\text{Gamma}[4/3] \times 9^{1/3}\left(\frac{Dx}{\gamma}\right)^{1/3}} c_{\text{bulk}} \qquad (6)$$

where Gamma[ ] is the Gamma function, D is the diffusivity of the polymer in bulk solution, x is the position of the probing spot in the axial direction, γ is the shear rate, c_b is the concentration of polymer in the bulk, and Γ is the polymer excess surface concentration. The shear rate γ for a laminar rectangular slit flow cell is given by

$$\gamma = \frac{6Q}{h^2 w} \qquad (7)$$

where Q is the flow rate, h is the height of the rectangular slit, and w is the width. The following values were used in the calculation:

$$Q = 1.67\ \text{cm}^3\ \text{s}^{-1} \qquad D = 30 \times 10^{-11}\ \text{m}^2\ \text{s}^{-1}$$
$$h = 0.025\ \text{cm} \qquad x = 0.040\ \text{m}$$
$$w = 1.4\ \text{cm} \qquad c_{\text{bulk}} = 460\ \mu\text{mol m}^{-3}$$

Convective−Diffusive Model. Assuming laminar flow and fully developed hydrodynamic conditions, a material balance over the fluid phase yields the following set of equations:[4]

$$v_z = 4v_{\max}\left(1 - \frac{y}{h}\right)\frac{y}{h} \qquad (8)$$

$$\frac{\partial c}{\partial t} + v_z \frac{\partial c}{\partial z} = D\left(\frac{\partial^2 c}{\partial y^2} + \frac{\partial^2 c}{\partial z^2}\right) \qquad (9)$$

Initial Condition:

$$c(z,y,0) = 0, \quad t = 0 \qquad (10)$$

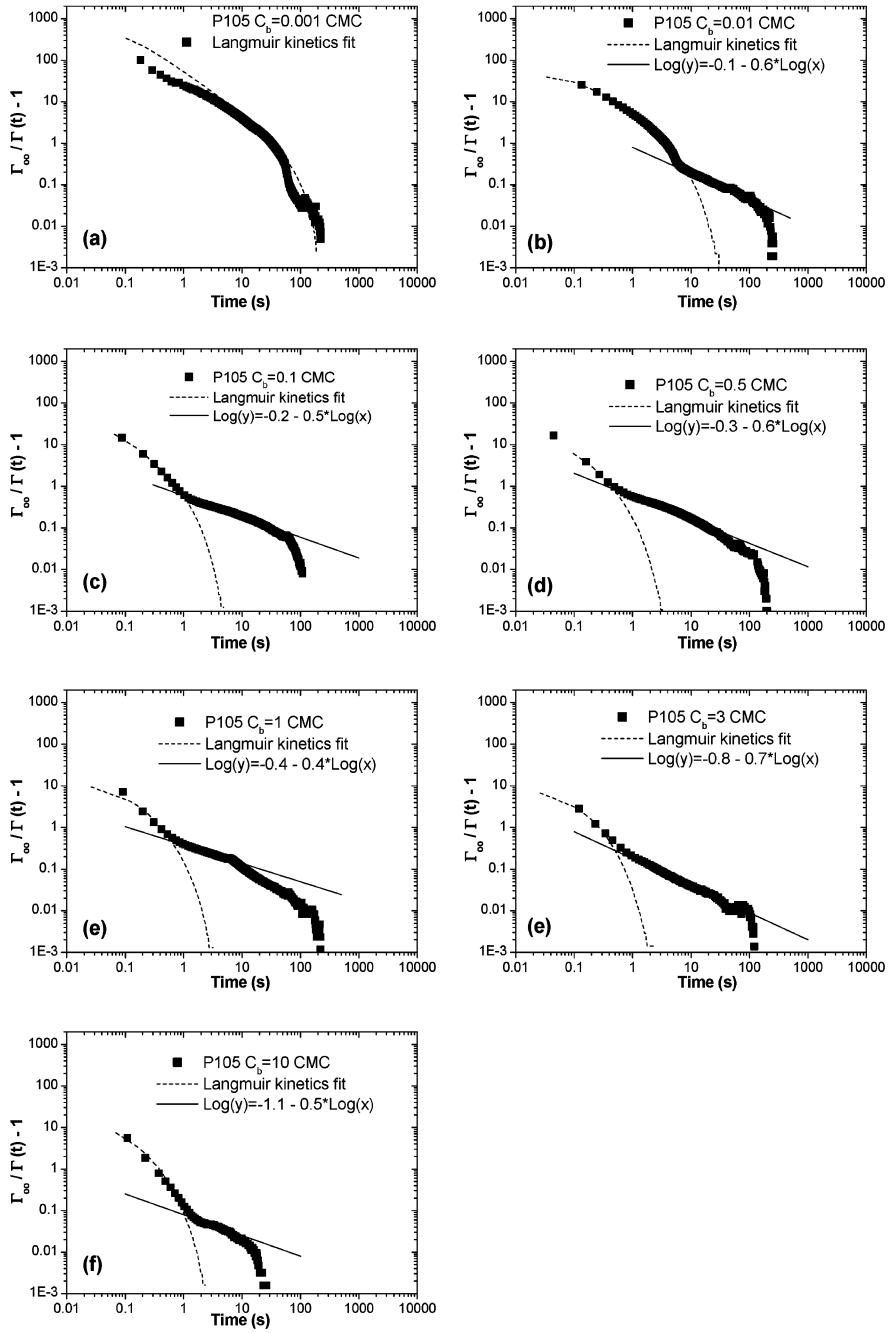

Figure 9. Comparison of the experimentally observed kinetics with the predictions of a Langmuir kinetics model (dashed curve) corrected to account for the effects of mass transfer for P105 ($E_{37}P_{56}E_{37}$) at (a) 0.001, (b) 0.01, (c) 0.1, (d) 0.5, (e) 1, (f) 3, and (g) 10 cmc concentration in the bulk solution. The solid line in each case highlights intermediate time asymptotic behavior. Plots are on a log−log scale.

Boundary Conditions:

$$D\frac{\partial c}{\partial y} = 0, \quad y = h \tag{11}$$

$$D\frac{\partial c}{\partial y} = \frac{\partial \Gamma}{\partial t}, \quad y = 0 \tag{12}$$

$$c(0,y,t) = c_{\text{in}}, \quad z = 0 \tag{13}$$

$$\frac{\partial c}{\partial z} = 0, \quad z = L \tag{14}$$

where z is the axis parallel to the direction of the flow and y is the axis perpendicular to the adsorbing surface. Equation 12 expresses the continuity of the first derivative of the concentration profile across the exit boundary as discussed by Danckwerts.[10]

A material balance at the solid surface yields

$$\frac{\partial \Gamma}{\partial t} = \Psi(c(z,0), \Gamma, ...), \quad y = 0 \tag{15}$$

where the function Ψ characterizes the intrinsic kinetics of the adsorption process. In our modeling we have used a Langmuirian expression:

$$\Psi = k_a c(z,0)(\Gamma_{\max} - \Gamma) - k_d\Gamma \tag{16}$$

The above system of equations can be recast in a dimensionless form by defining the following variables:

$$\hat{z} = \frac{z}{L} \qquad \hat{k}_a = k_a c_{in} \frac{L}{v_{max}}$$

$$\hat{y} = \frac{y}{h} \qquad \hat{k}_d = k_d \frac{L}{v_{max}}$$

$$\hat{t} = t \frac{v_{max}}{L} \qquad \hat{\Gamma} = \frac{\Gamma}{\Gamma_{max}}$$

$$\hat{c} = \frac{c}{c_{in}} \tag{17}$$

For the fluid phase we obtain

$$\frac{\partial \hat{c}}{\partial \hat{t}} + 4\hat{y}(1-\hat{y})\frac{\partial \hat{c}}{\partial \hat{z}} = \frac{1}{Pe}\left(\left(\frac{L}{h}\right)^2 \frac{\partial^2 \hat{c}}{\partial \hat{y}^2} + \frac{\partial^2 \hat{c}}{\partial \hat{z}^2}\right) \tag{18}$$

Initial Condition:

$$\hat{c}(\hat{z},\hat{y},0) = 0, \quad \hat{t} = 0 \tag{19}$$

Boundary Conditions:

$$\frac{\partial \hat{c}}{\partial \hat{y}} = 0, \quad \hat{y} = 1 \tag{20}$$

$$\frac{1}{Pe}\left(\frac{L}{h}\right)\left(\frac{L c_{in}}{\Gamma_{max}}\right)\frac{\partial \hat{c}}{\partial \hat{y}} = \frac{\partial \hat{\Gamma}}{\partial \hat{t}}, \quad \hat{y} = 0 \tag{21}$$

$$\hat{c}(0,\hat{y},\hat{t}) = 1, \quad \hat{z} = 0 \tag{22}$$

$$\frac{\partial \hat{c}}{\partial \hat{z}} = 0, \quad \hat{z} = 1 \tag{23}$$

and for the solid surface

$$\frac{\partial \hat{\Gamma}}{\partial \hat{t}} = \hat{k}_a \hat{c}(\hat{z},0,\hat{t})(1-\hat{\Gamma}) - \hat{k}_d \hat{\Gamma} \tag{24}$$

where *Pe* is the Peclet number given by the quantity $v_{max}L/D$. In our experiments *Pe* is $O(10^9)$. Given that the ratio L/h is very high, it is customary to drop the axial dispersion term (the second derivative of c with respect to z) as its contribution becomes negligible; the second axial boundary condition (23) is also dropped. The integration of this scheme has been implemented with the gPROMS package (Process Systems Enterprise Ltd., London, United Kingdom).

Fitting Procedure. We have fixed the value of the diffusivity D at 30×10^{-11} m^2/s. We chose this value based on the micellar diffusivity data of Nolan et al.,[26] and we used the inverse diameter relationship of the Stokes−Einstein equation to adjust the value to a single polymer chain diffusivity. We assumed a ratio of 10 between micellar and single polymer chain sizes. Given the limited scope of this study, we made no further attempts at incorporating micellar contributions in the diffusivity or in the form of the kinetics functions, but the interested reader is referred to the work of Bijsterbosch et al.[3] for an example of how to deal with these issues.

For determining the rate parameters, we modified the forward rate $\hat{k}_a$ until the initial rate slope matched the experimental value (at $\hat{t} = 0$, $\hat{\Gamma} = 0$, and $\partial\hat{\Gamma}/\partial\hat{t} = \hat{k}_a\hat{c}(\hat{z},0,0)$). We then modified the backward rate $\hat{k}_d$ until we matched the coverage at infinite time (at equilibrium). Generally, we found that $\hat{k}_d$ values obtained in the adsorption data fit and values obtained in fits of the desorption data did not agree. This mismatch is a reflection of the non-Langmuirian nature of the kinetics.

Acknowledgment. The National Science Foundation (NSF) under Award DMR-9808677 funded this work. P. Brandani acknowledges additional support through a NSF fellowship from the NEAT-IGERT program (IGERT Grant DGE-9972741). We thank Professor Stefano Brandani of University College London (United Kingdom) for providing access to his laboratory and for introducing us to the gPROMS package.

Note Added after ASAP Posting

This article was inadvertently posted without corrections on 10/30/2003. The corrected version was posted on 11/14/2003. An additional correction was made in the Fitting Procedure. The units for diffusivity were changed from μmol/m^2 to m^2/s. The corrected version was posted 11/20/03.

References and Notes

(1) Ahmed, F.; Alexandridis, P.; Neelamegham, S. *Langmuir* **2001**, *17*, 537.
(2) Alexandridis, P.; Holzwarth, J. F.; Hatton, T. A. *Macromolecules* **1994**, *27*, 2414.
(3) Bijsterbosch, H. D.; Stuart, M. A. C.; Fleer, G. J. *Macromolecules* **1998**, *31*, 9281.
(4) Bird, R. B.; Stewart, W. E.; Lightfoot, E. N. *Transport Phenomena*; Wiley: New York, 1960.
(5) Born, M. *Principles of Optics*, 6th ed.; Pergamon Press: Oxford, 1980; p 58.
(6) Brandani, P.; Stroeve, P. *Macromolecules* **2003**, *36*, 9492.
(7) Chakraborty, A. K.; Golumbfskie, A. J. *Annu. Rev. Phys. Chem.* **2001**, *52*, 537.
(8) Cohen-Stuart, M. A. Macromolecular Adsorption: A Brief Introduction. In *Biopolymers at Interfaces*; Malmsten, M., Ed.; Marcel Dekker: New York, 1998; Vol. 75, pp 1−25.
(9) Creager, S. E.; Clarke, J. *Langmuir* **1994**, *10*, 3675.
(10) Danckwerts, P. V. *Chem. Eng. Sci.* **1953**, *2*, 1.
(11) De Feijter, J. A.; Benjamins, J.; Veer, F. A. *Biopolymers* **1978**, *17*, 1759.
(12) Debruijn, H. E.; Altenburg, B. S. F.; Kooyman, R. P. H.; Greve, J. *Opt. Commun.* **1991**, *82*, 425.
(13) Eskilsson, K.; Tiberg, F. *Macromolecules* **1997**, *30*, 6323.
(14) Frantz, P.; Granick, S. *Macromolecules* **1994**, *27*, 2553.
(15) Fu, Z. G.; Santore, M. M. *Colloids Surf., A* **1998**, *135*, 63.
(16) Fu, Z. L.; Santore, M. M. *Macromolecules* **1998**, *31*, 7014.
(17) Green, R. J.; Tasker, S.; Davies, J.; Davies, M. C.; Roberts, C. J.; Tendler, S. J. B. *Langmuir* **1997**, *13*, 6510.
(18) Hansen, W. N. *J. Opt. Soc. Am.* **1968**, *58*, 380.
(19) Huang, Y. W.; Gupta, V. K. *Macromolecules* **2001**, *34*, 3757.
(20) Johner, A.; Joanny, J. F. *Macromolecules* **1990**, *23*, 5299.
(21) Knoll, W. *Annu. Rev. Phys. Chem.* **1998**, *49*, 569.
(22) Lévêque, M. *Ann. Mines* **1928**, *13*, 284.
(23) Lok, K. B.; Cheng, Y.; Robertson, C. R. *J. Colloid Interface Sci.* **1983**, *91*, 104.
(24) Malmsten, M.; Tiberg, F. *Langmuir* **1993**, *9*, 1098.
(25) Muthukumar, M.; Ober, C. K.; Thomas, E. L. *Science* **1997**, *277*, 1225.
(26) Nolan, S. L.; Phillips, R. J.; Cotts, P. M.; Dungan, S. R. *J. Colloid Interface Sci.* **1997**, *191*, 291.
(27) Peppas, N. A.; Langer, R. *Science* **1994**, *263*, 1715.
(28) Tiberg, F.; Landgren, M. *Langmuir* **1993**, *9*, 927.

MA034268X